Supplementary Information

I. Supplementary Figures

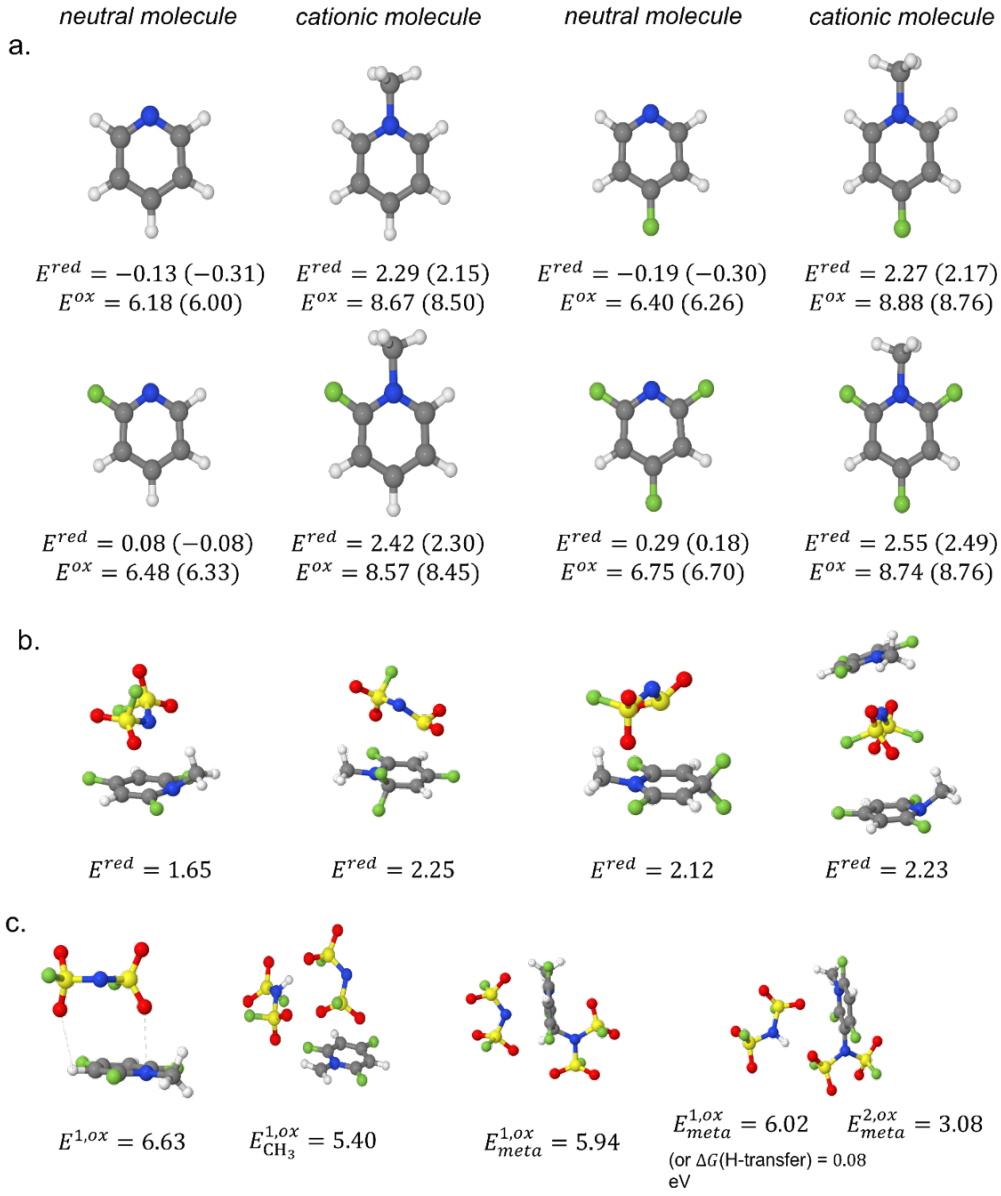

Figure S1. a. Reduction and oxidation potentials of different neutral and cationic additives immersed in implicit solvent (ether, ε=4.24) modeled using polarized continuum model (PCM) in V vs. Li/Li^+ from G4MP2 composite quantum chemical calculations and wB97XD/6-31+G(d,p) DFT calculations (in parentheses). **b.** Reduction potentials of N-methyl-2,4,6-trifluoropyridinium FSI complexes in V vs. Li/Li^+ from PCM(ether)/wB97XD/6-31+G(d,p) DFT calculations. **c.** Oxidation potentials of N-methyl-2,4,6-trifluoropyridinium FSI complexes in V vs. Li/Li^+ from PCM(ether)/wB97XD/6-31+G(d,p) DFT calculations. A 1 or 2 in the superscript of the oxidation potentials indicates whether the potential corresponds to the 1st or 2nd oxidation. CH_3 or meta in the subscript refers to the carbon involved in the oxidation reaction with FSI. Oxidation coupled with H-transfer from the CH_3 to FSI gives the lowest potential. Two other oxidation reactions are reported near 6 V where oxidation is coupled with *meta*-C-N(FSI) bond formation and (at a slightly higher potential/with a small barrier) H-transfer from the sp^3 hybridized carbon to the second FSI. Taking this species (after H-transfer) as an activated state, a second oxidation occurs at 3.08 V.

.

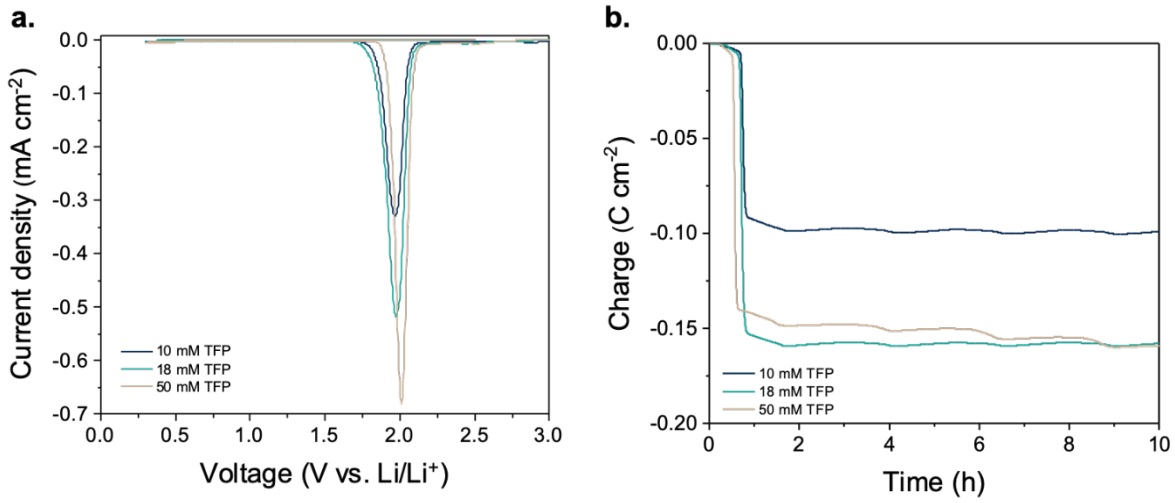

Figure S2. a. First cycle CV profiles collected in DME + 1 M LiFSI electrolytes with different concentrations of fluorinated cation at a 1 mm Cu disk working electrode using a 0.5 mV s^{-1} scan rate and a voltage window of 0.3 – 3.0 V vs. Li/Li^+ **b.** Specific charge versus time graph from the first cycle CV profiles.

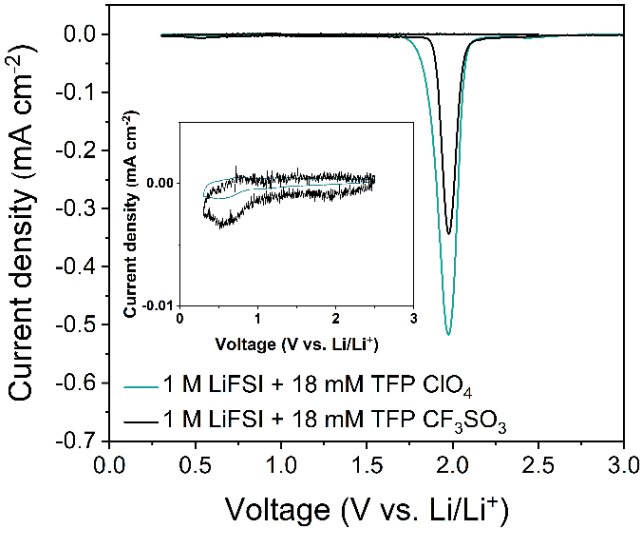

Figure S3. First and second (inset) cycle CV profiles collected in DME + 1 M LiFSI electrolytes with 18 mM TFP ClO_4 and with 18 mM TFP CF_3SO_3 using a 1 mm Cu disk working electrode at a 0.5 mV s^{-1} scan rate and a voltage window of 0.3 – 2.5 V vs. Li/Li^+.

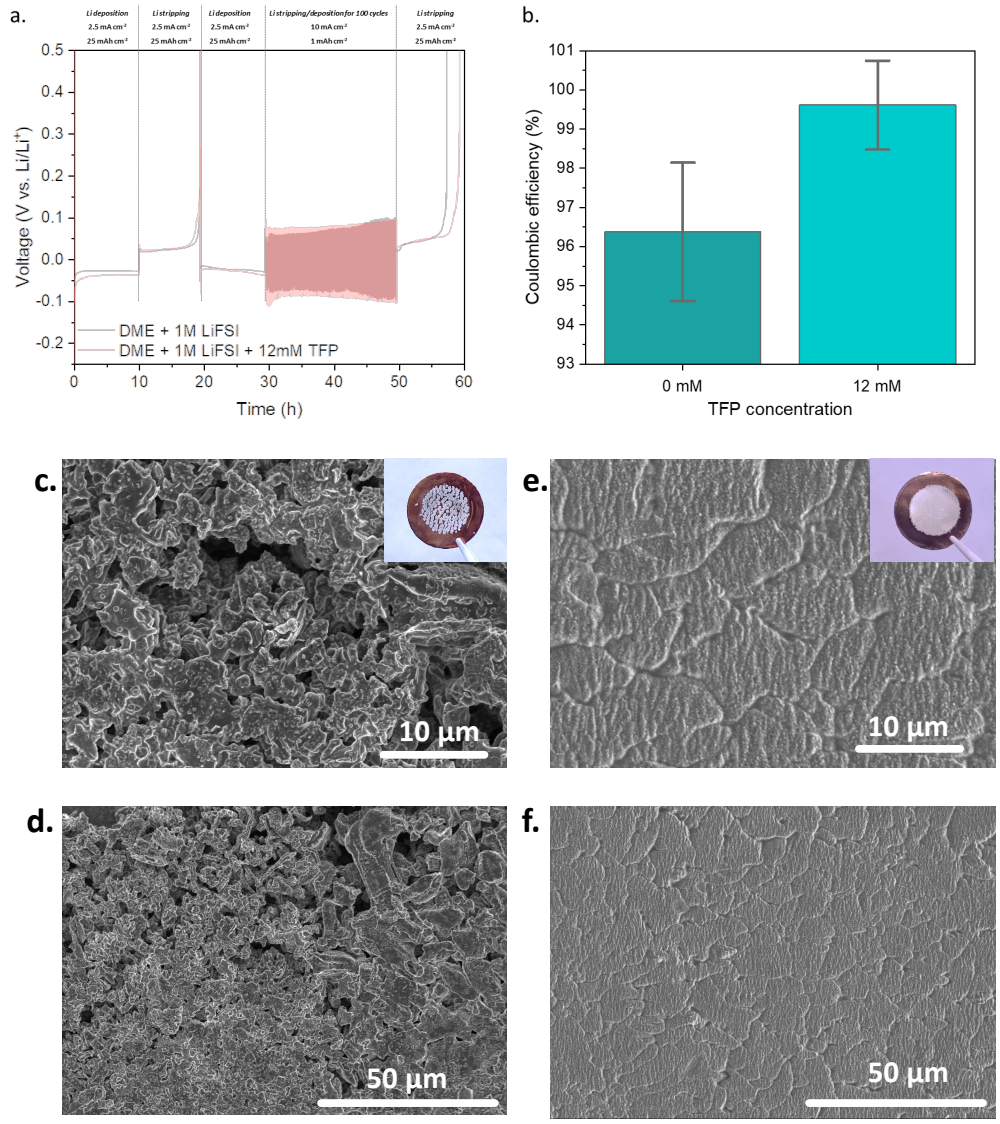

Figure S4. a. Aurbach coulombic efficiency test using different electrolytes. Asymmetric Cu // Li coin cells were assembled with different electrolytes and Li plating and stripping was done for 100 times with the current density of 10 mA cm^{-2} with areal loading of 1 mAh cm^{-2} prior to excess deposition of Li (25 mAh cm^{-2} with current density of 2.5 mA cm^{-2}). **b.** Bar graph representing the average coulombic efficiencies of 5+ cells with 1M LiFSI in DME (96.4 %) and 1M LiFSI in DME + 12 mM TFP (99.6 %), respectively. **c.-d.** Digital photographs (inset) and SEM images of the unidirectionally deposited Li metal in 1 M LiFSI (Solvionic) in DME; **e.-f.** Digital photographs (inset) and SEM images of the unidirectionally deposited Li metal in 12 mM TFP + 1M LiFSI in DME.

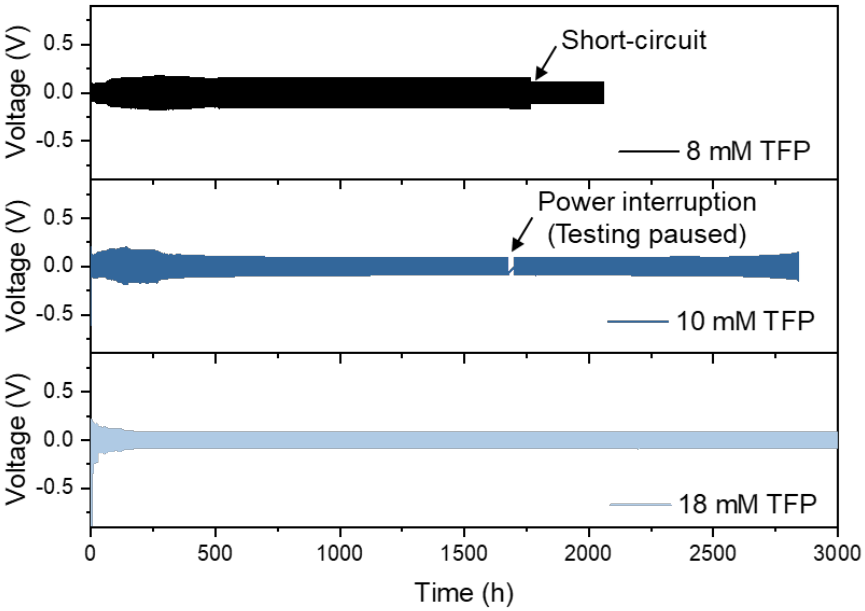

Figure S5. Galvanostatic cycling of a Li^0-Li^0 symmetric cell at 10 mA cm^{-2} using 1 M LiFSI in DME as an electrolyte with different concentration of TFP.

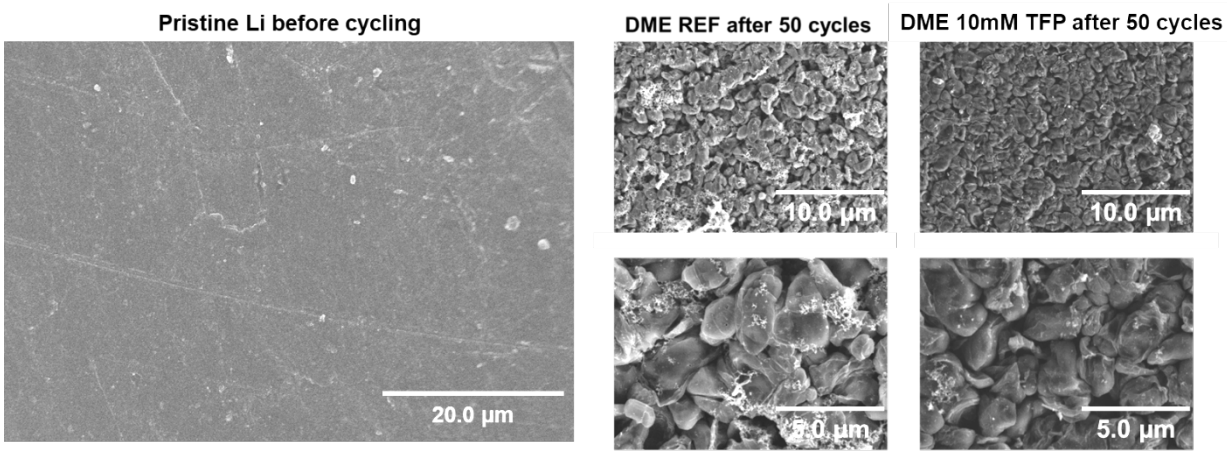

Figure S6. SEM images of the pristine and 50 times cycled Li metal electrode. Galvanostatic cycling of a Li^0-Li^0 symmetric cell at 10 mA cm^{-2} was used with 1 M LiFSI in DME for the reference sample and 1 M LiFSI in DME with 10 mM of TFP for the additive added sample.

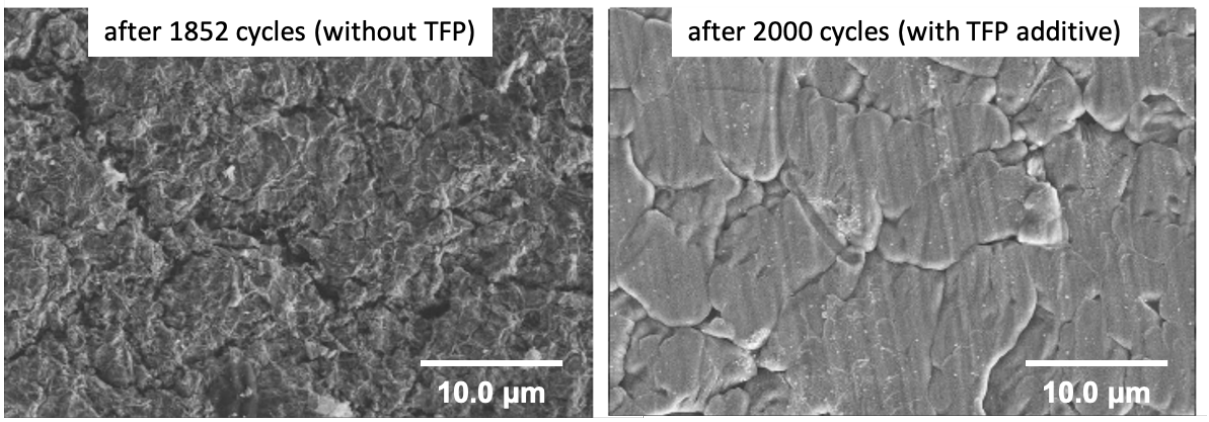

Figure S7. SEM images of the long-term cycled Li metal electrode. **a.** Galvanostatic cycling of a Li^0-Li^0 symmetric cell at 10 mA cm^{-2} was used with 1 M LiFSI in DME for the reference sample and **b.** DME 1 M LiFSI + 10 mM TFP for the additive-containing sample.

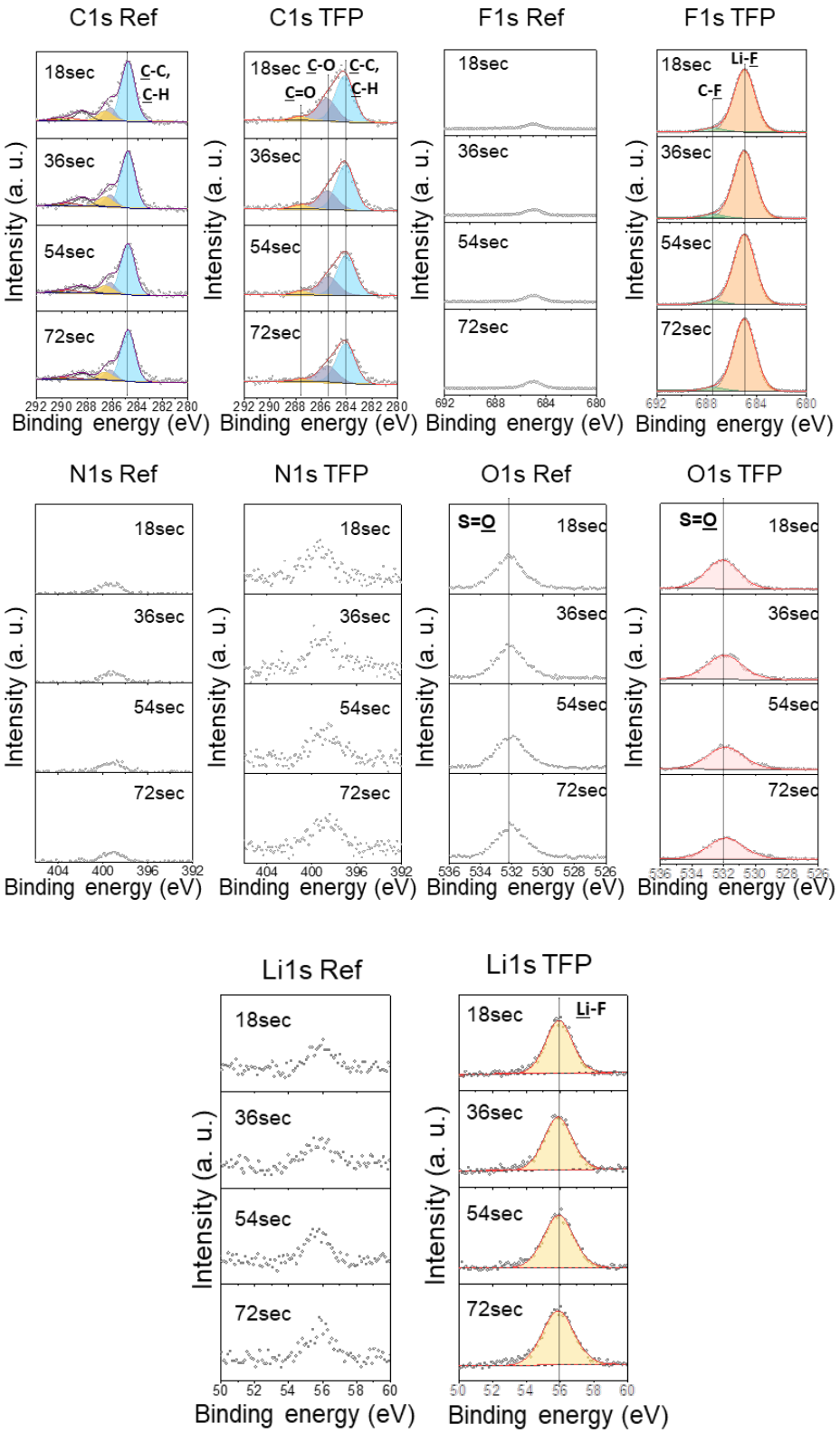

Figure S8. XPS C 1s, F 1s, Li 1s, N 1s and O 1s spectra of SEI layer formed on Cu electrodes cycled in DME + 1 M LiFSI reference electrolyte and DME + 1 M LiFSI with 18 mM TFP (estimated depth: 0.5 nm, 1.0 nm, 1.5 nm and 2.0 nm for 18 s, 36 s, 54 s and 72 s, respectively). Samples were prepared by performing 10 cycles of cyclic voltammetry using an electrochemical cell consisting of Cu||Li||Ag/AgCl with 0.5 mV s^{-1} scan rate within the voltage of 0.3 – 2.5 V vs. Li/Li^{+}.

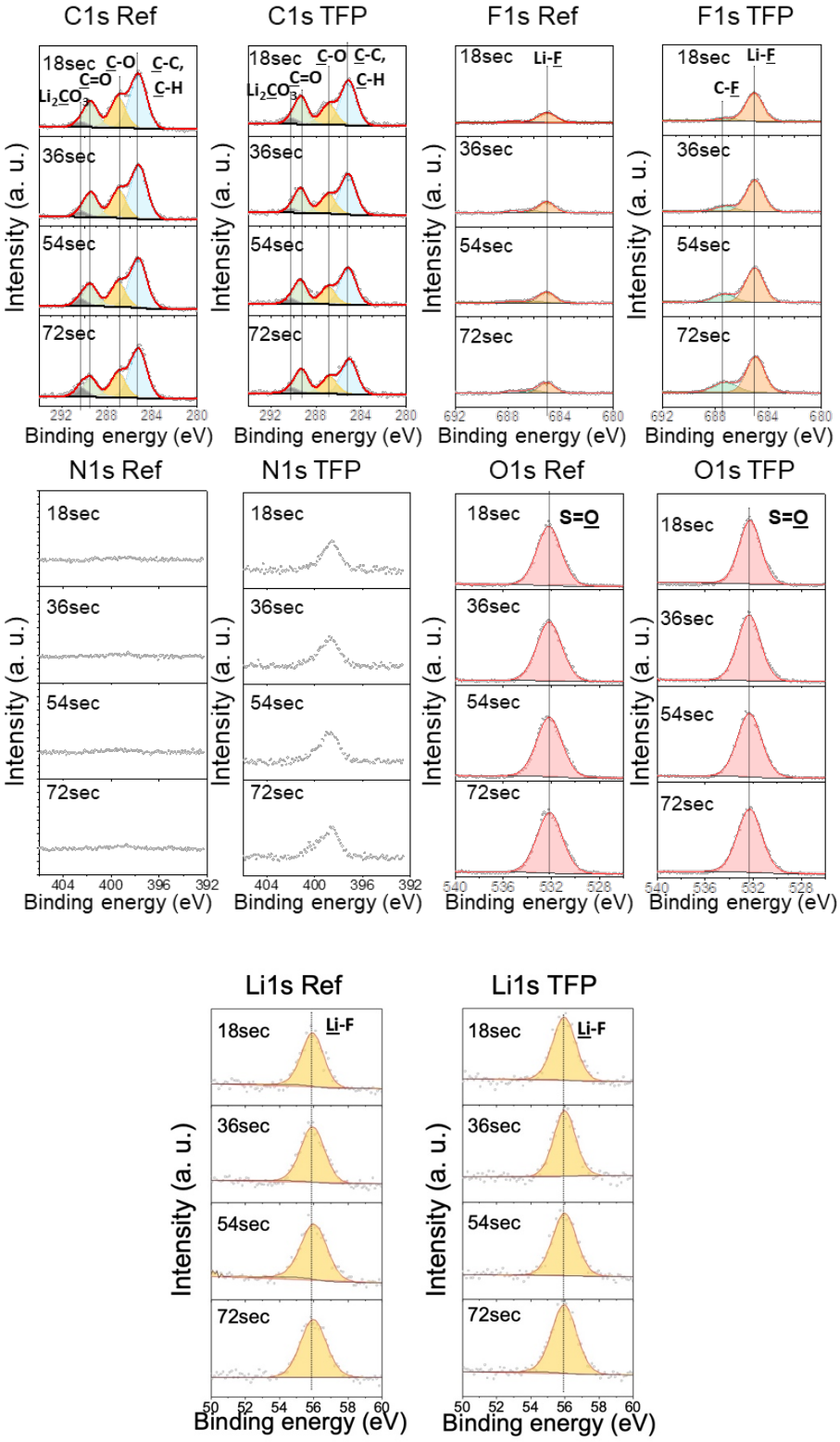

Figure S9. XPS C 1s, F 1s, Li 1s, N 1s and O 1s spectra of SEI layer formed on cycled Li electrodes in DME + 1M LiFSI reference electrolyte and DME + 1M LiFSI + 18 mM TFP (estimated depth: 0.5 nm, 1.0 nm, 1.5 nm and 2.0 nm for 18 s, 36 s, 54 s and 72 s, respectively). Samples were prepared by performing 25 galvanostatic charge-discharge cycles (0.1C and 1C rate for three and 22 cycles, respectively) using a coin cell consisting of NCM811||Li.

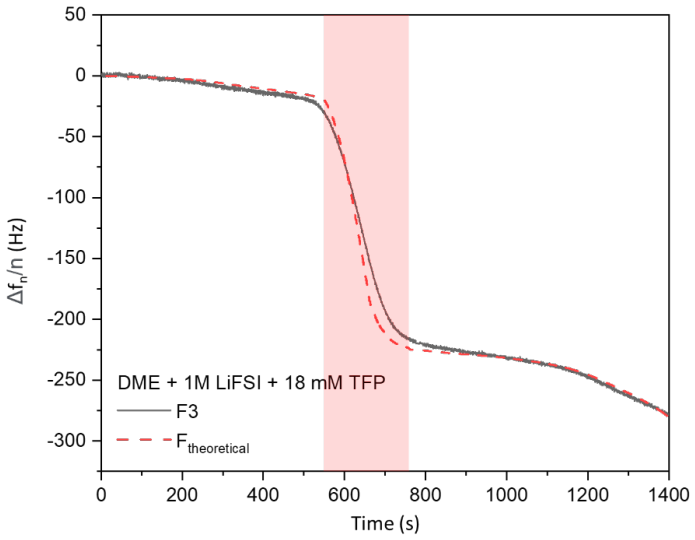

Figure S10. Frequency change versus time using EQCM-D analysis for DME + 1 M LiFSI + 18 mM TFP. The theoretical frequency change versus time was calculated using Sauerbrey equation for the highlighted region.

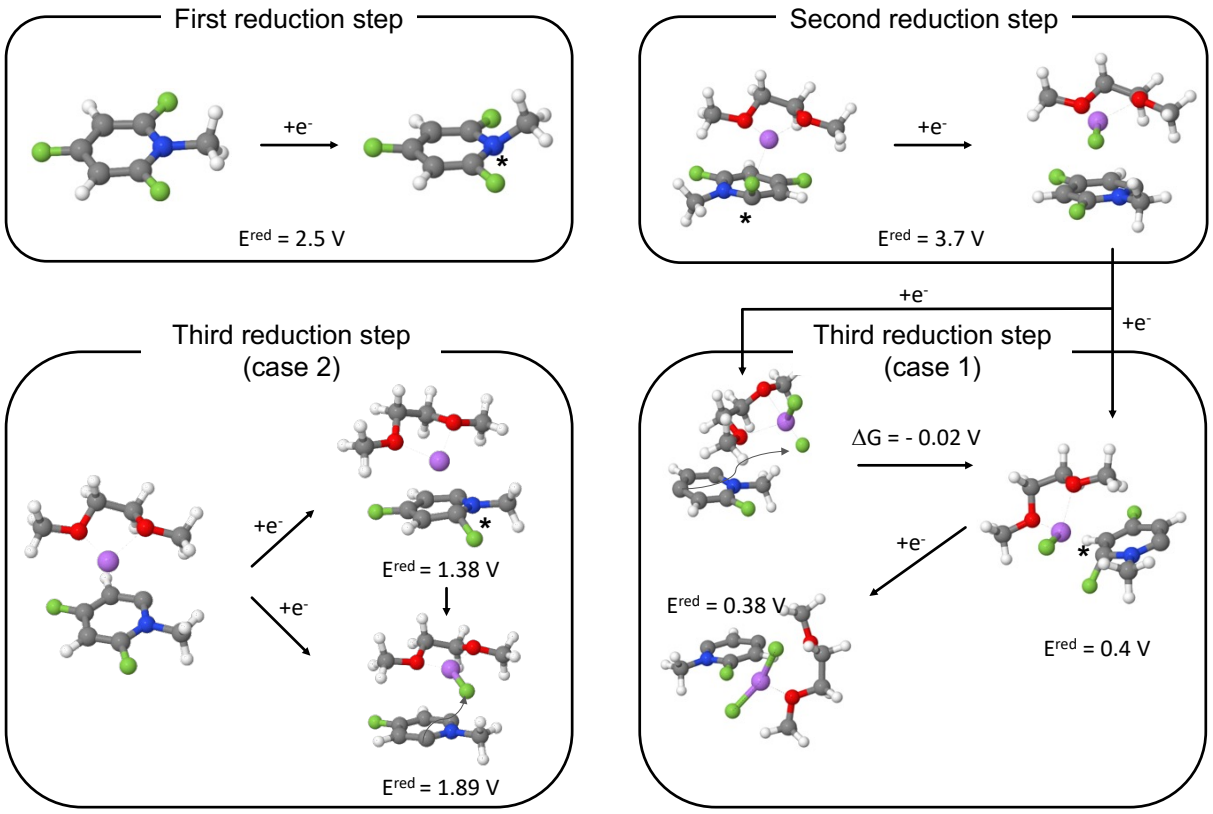

Figure S11. Reduction and decomposition reaction of the TFP - Li^+(DME) complexes in implicit solvent modeled using polarized continuum model PCM (ether) in V vs. Li/Li^+ from wB97XD/6-31+G(d,p) DFT calculations.

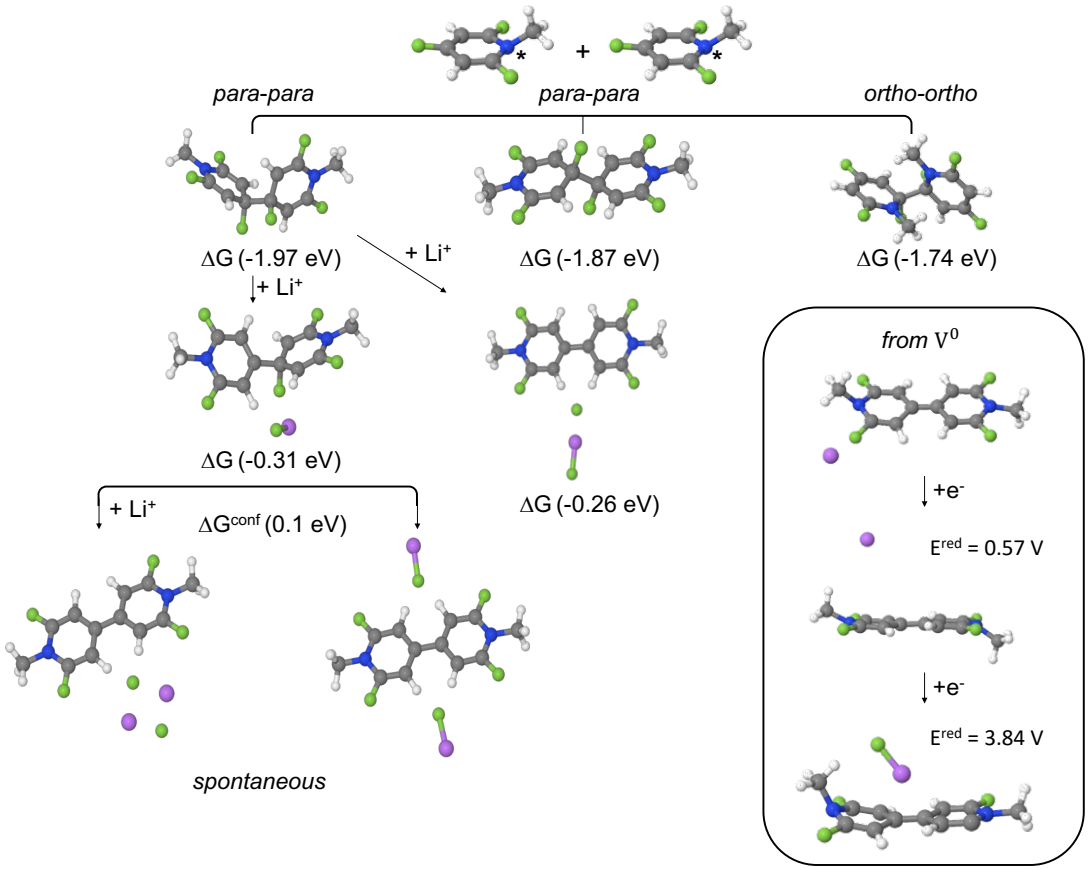

Figure S12. Reaction cascade resulting from the combination of two TFP radical species after their 1st reductions (both species are reduced, the radical is denoted by an asterisk). Reaction free energies (in eV) are reported at the PCM(ether)/wB97XD/6-31+G(d,p) level of theory. The reduction potentials are reported at the same level of theory with units of V vs Li/Li^+. In the box on the right hand side of the figure, 'from V^{0}' indicates that the viologen species depicted has a neutral charge.

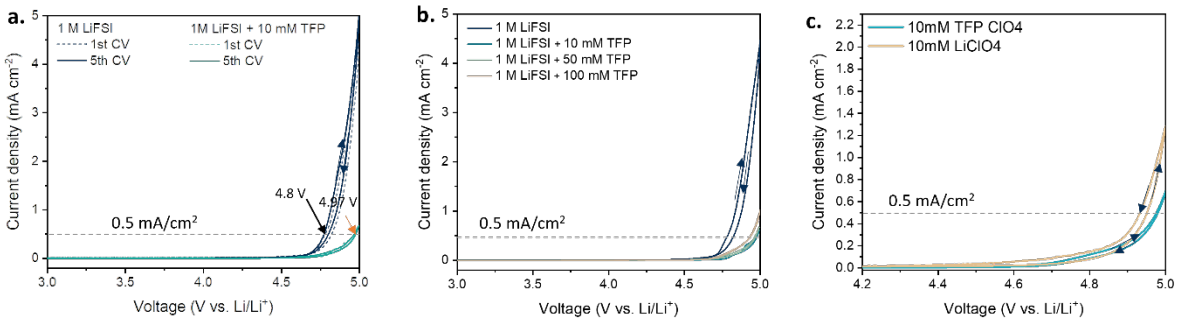

Figure S13. Oxidative stability of DME-based electrolytes with TFP. CV was measured in the potential range from 3.0 V to 5.0 V (vs. Li/Li^+) on an Au disk electrode with a scan rate of 0.5 mV/s. **a.** comparison between 1M LiFSI in DME, 1M LiFSI in DME with 10 mM $LiClO_4$ and 1M LiFSI in DME with 10 mM TFP ClO_4. **b.** oxidative stability test with different TFP concentration. **c**. 1M LiFSI in DME with 10 mM $LiClO_4$ and 1M LiFSI in DME with 10 mM TFP ClO_4.

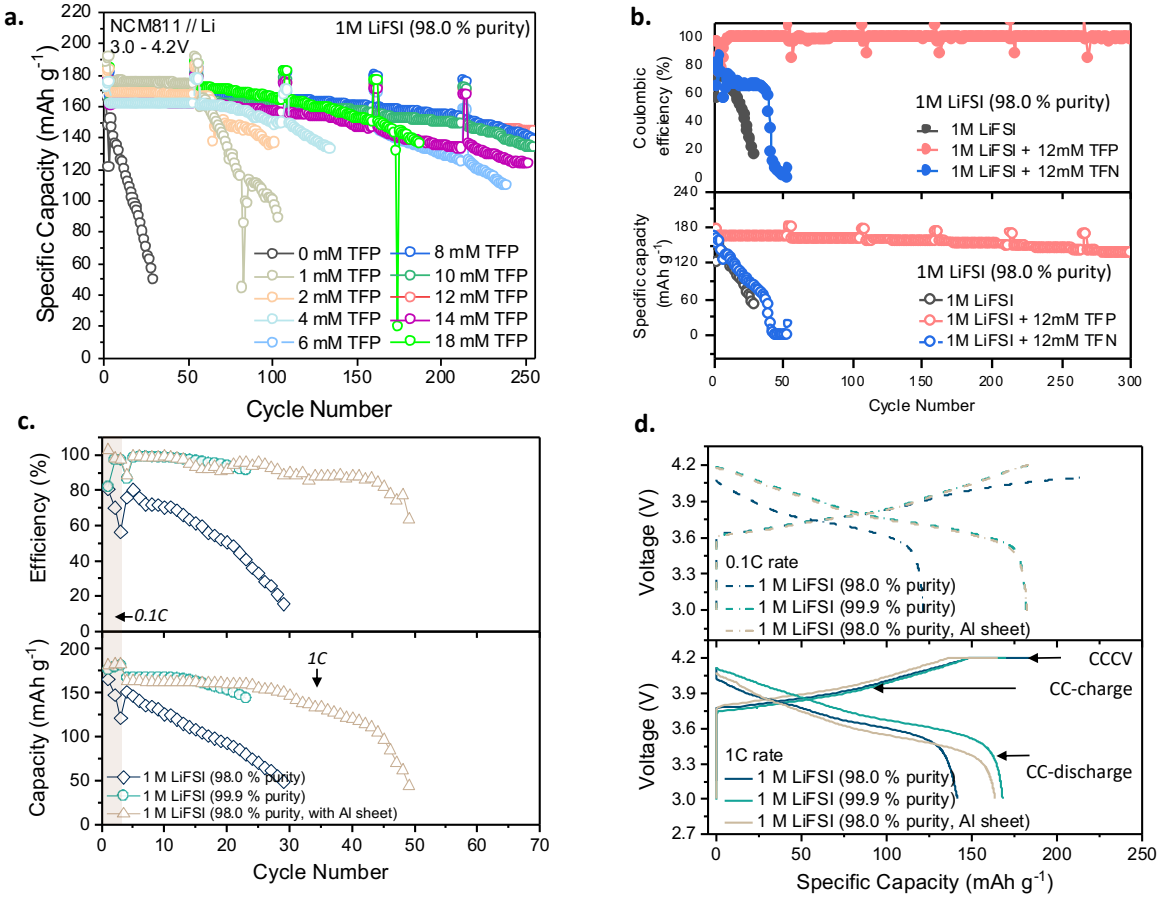

Figure S14. a. Long-term cycling results of NCM811|| 250 µm Li full cells with different TFP concentrations (0.1C-rate for three cycles and 1C-rate for 50 cycles in a loop) in 1M LiFSI (98.0 % purity). **b.** Long-term cycling results of NCM811/Li full cells without additive, with 12mM TFP (cation) and 12mM TFN (neutral). **c-d:** NCM811||250 µm Li cycling data (**c**) and respective charge discharge profiles (**d**) collected in reference electrolyte with LiFSI salt of different purity level and with and without an additional Al sheet underneath NCM811 cathode.

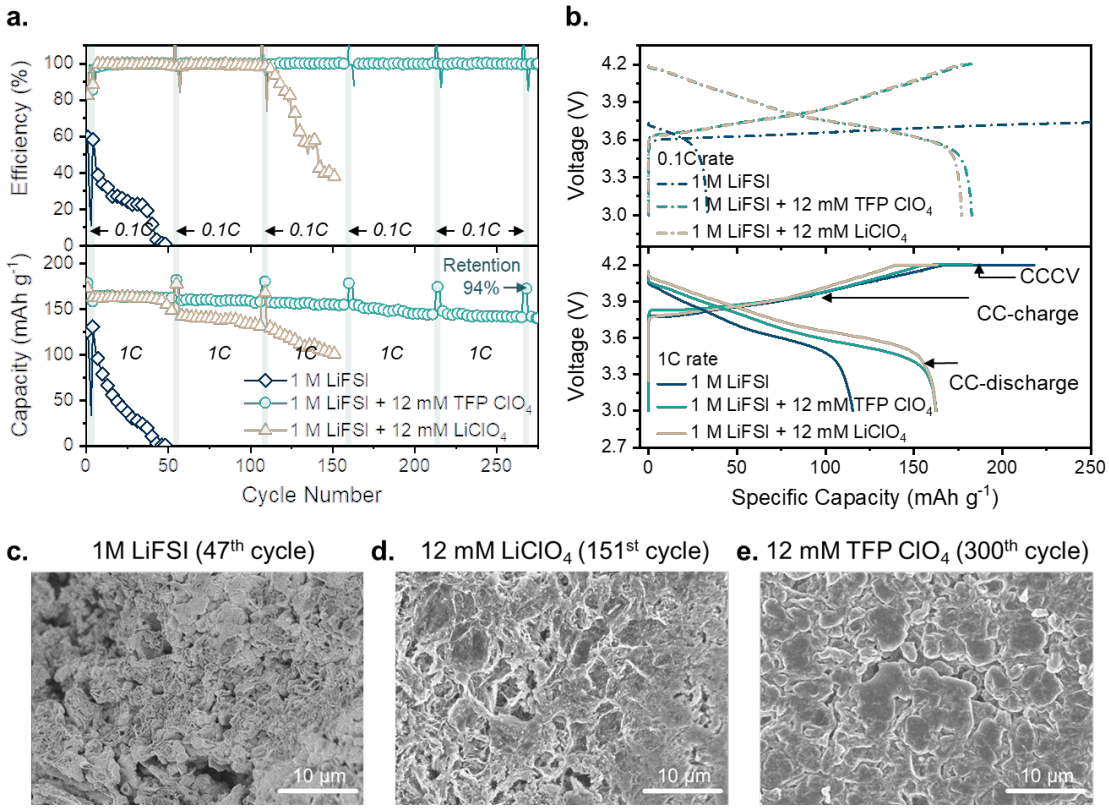

Figure S15. a. NCM811||50 µm Li full cell cycle data, **b**. voltage profile from full cell cycle data, and **c-e.** SEM image of anode at end-of-life cycle using 1 M LiFSI in DME, 1 M LiFSI in DME + 12 mM $LiClO_4$ and 1 M LiFSI in DME + 12 mM TFP ClO_4

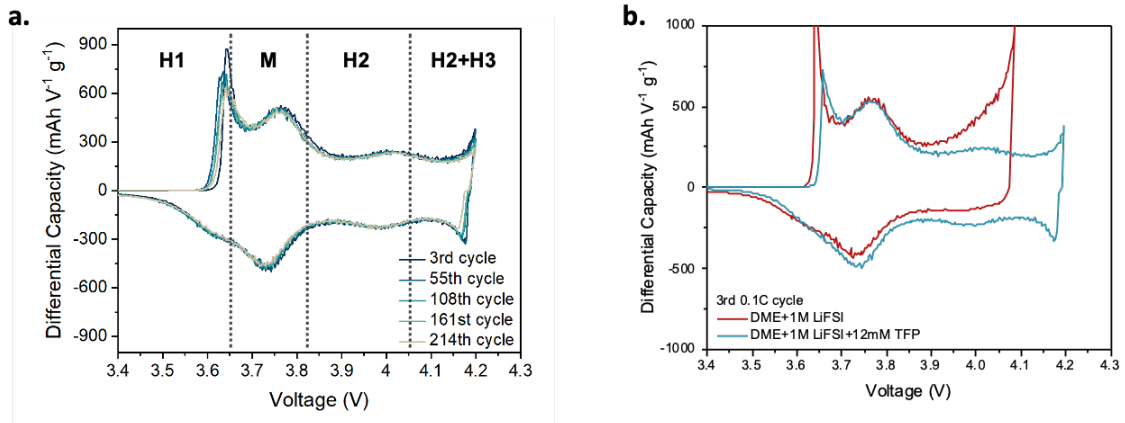

Figure S16. Differential capacity profiles (dQ/dV) for NCM811|| 250 µm Li full cells with 1 M LiFSI in DME and 1 M LiFSI in DME with 12 mM TFP.

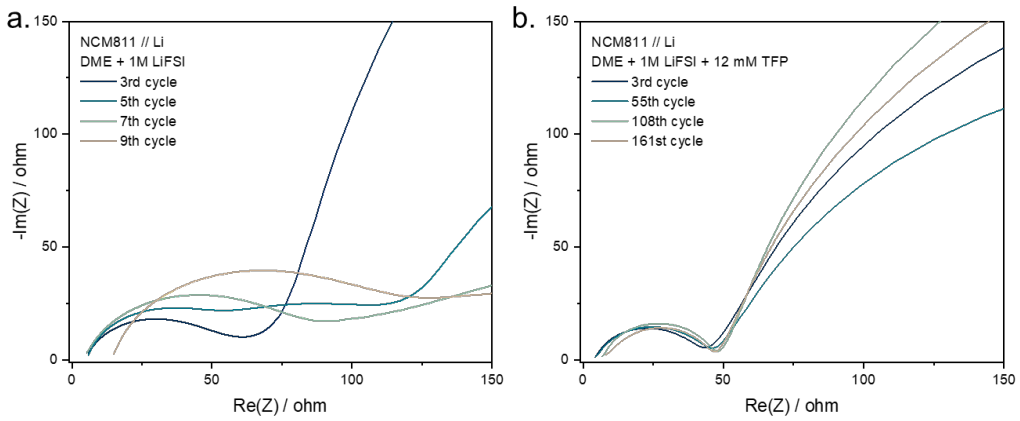

Figure S17. Electrochemical impedance spectroscopy (EIS) data for NCM811|| 250 µm Li full cells with **a.** 1 M LiFSI in DME or **b.** 1 M LiFSI in DME and 12 mM TFP.

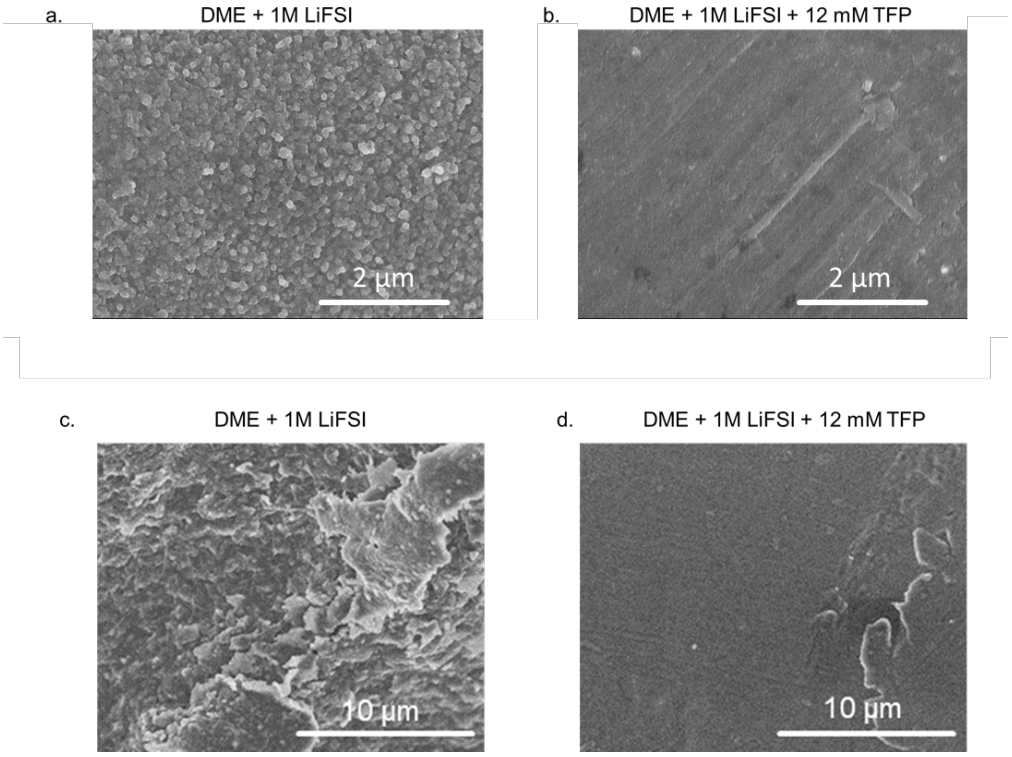

Figure S18. SEM images of the Al current collectors on NCM811 cathode material. **a.** using DME + 1M LiFSI with higher purity level (99.9 %, Solvionic) after 20 cycles at 1C. **b.** using DME + 1M LiFSI + 12 mM TFP with higher purity level (99.9 %, Solvionic) after 20 cycles at 1C. **c.** using DME + 1M LiFSI with lower purity level (98.0 %, TCI) after 20 cycles at 1C and **d.** using DME + 1M LiFSI + 12 mM TFP with lower purity level (98.0 %, TCI) after 160 cycles at 1C. The LiFSI salt from TCI Europe indicates 98% minimum purity. However, we discovered that there is a purity level deviation by different batches.

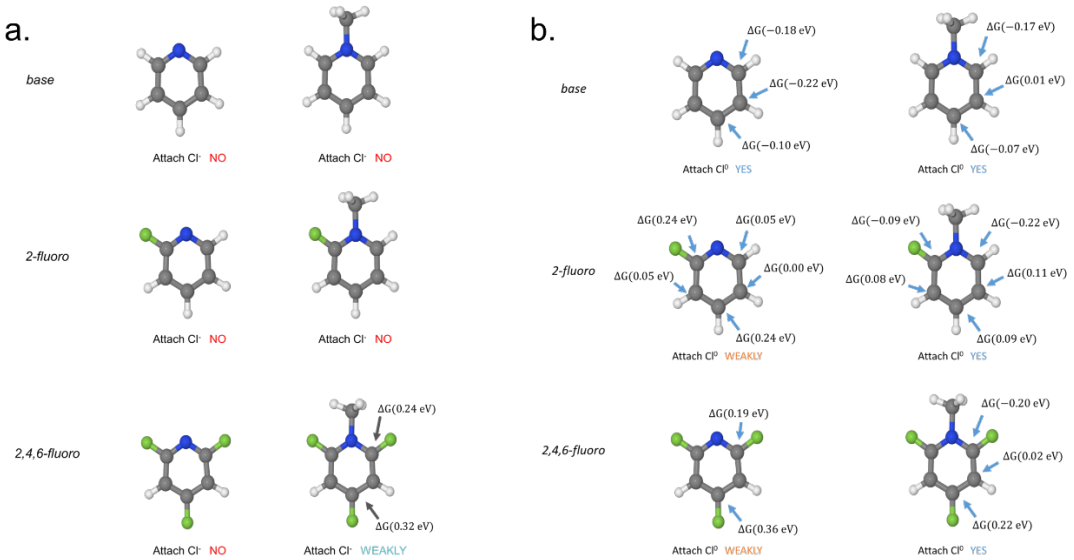

Figure S19. a. TFP cations Cl^- rom PCM (ether) from wB97XD/6-31+G(d,p) and MP2/aug-cc-pvQz DFT calculations. **b.** Reactivity of each species with Cl^0 (oxidized) or Cl^-. All calculations were performed with the PCM(ether)/wB97XD/6-31+G(d,p) model chemistry. The initial geometry is initialized with a C-Cl bond formed at each of the *symmetry-unique* ortho, meta, and para positions. Reaction free energies (in eV) are reported if and only if the C-Cl does not dissociate during optimization. 'No' indicates all C-Cl bonds dissociated, no energy is reported. 'Weakly' is used to describe formation of a stable compound but during an endergonic process. 'Yes' indicates at least one of the processes is exergonic.

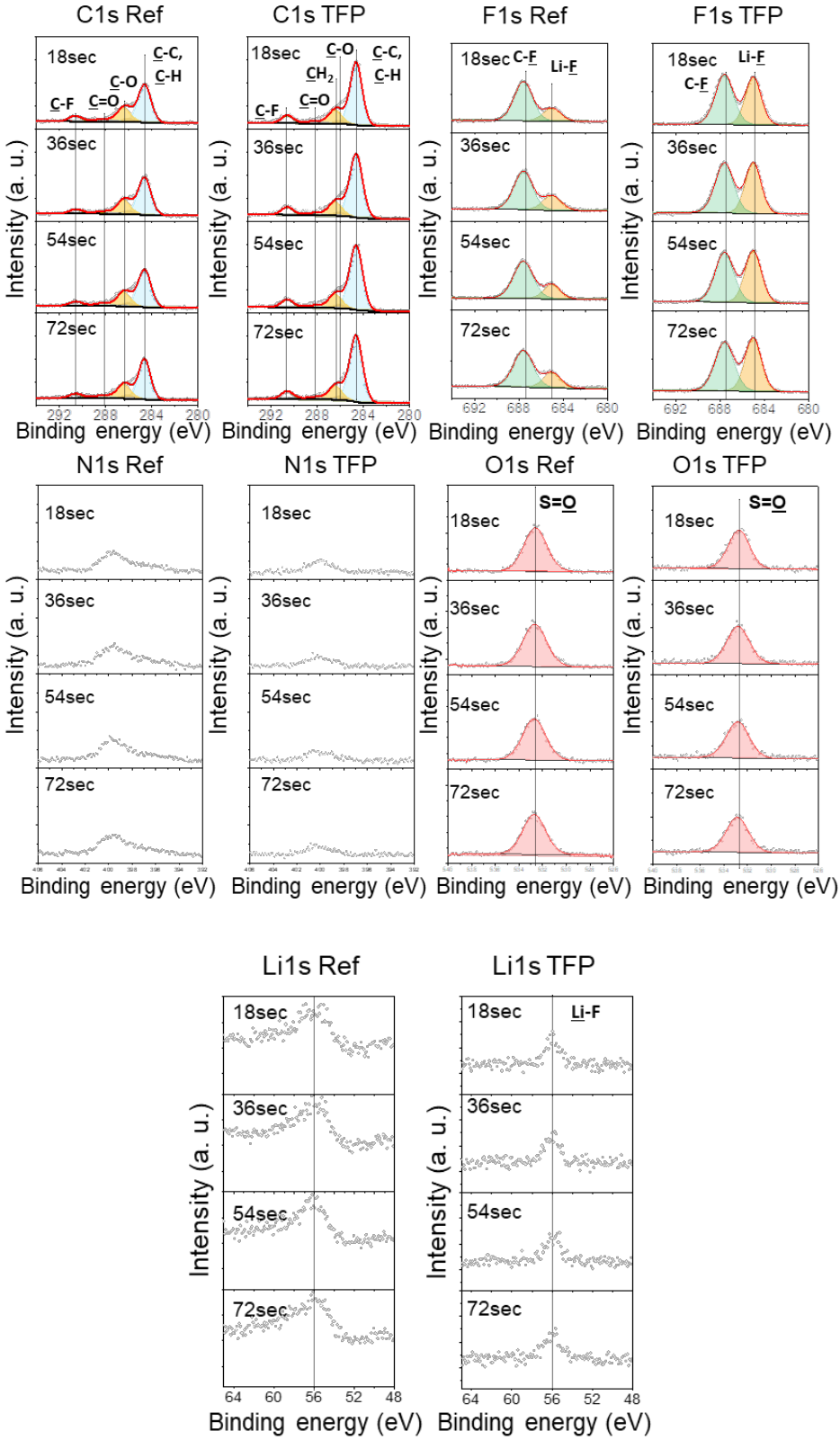

Figure S20. XPS C 1s, F 1s, Li 1s, N 1s and O 1s spectra of CEI layer formed on cycled NCM electrodes in DME + 1M LiFSI reference electrolyte and DME + 1M LiFSI with 12 mM TFP (estimated depth: 0.5 nm, 1.0 nm, 1.5 nm and 2.0 nm for 18 s, 36 s, 54 s and 72 s, respectively). Samples were prepared by performing 25 galvanostatic charge-discharge cycles (0.1C and 1C rate for three and 22 cycles, respectively) using a coin cell consisting of NCM811||Li.

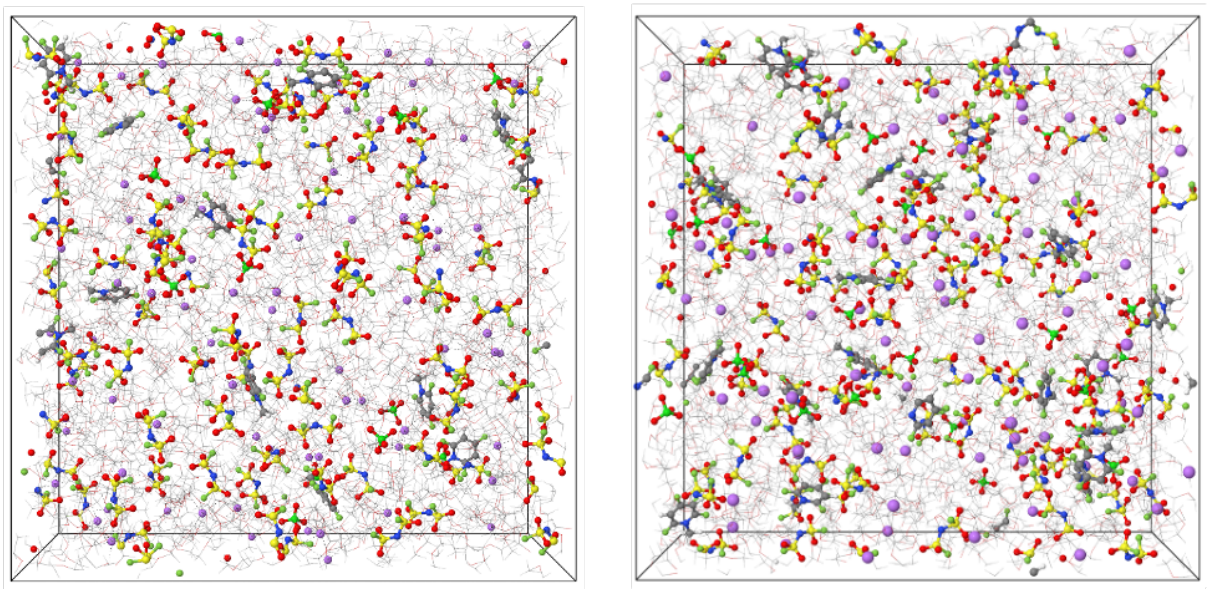

Figure S21. Snapshots of MD simulation cell for 0.91 M LiFSI and 0.14 M [TFP][ClO_4] in DME (left) and 0.91 M LiFSI and 0.27 M [TFP][ClO_4] in DME (right) at 298 K with DME solvent shown as transparent wireframe. Default jmol colors were used.

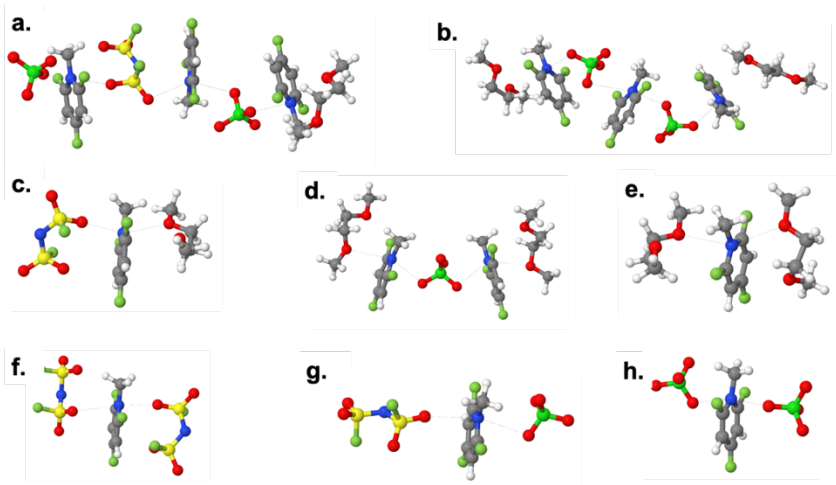

Figure S22. Representative TFP^+ solvates for 0.91 M LiFSI and 0.27 M [TFP][ClO_4] in DME at 298 K. Solvates include molecules within with 3.2 Å cutoff around TFP^+.

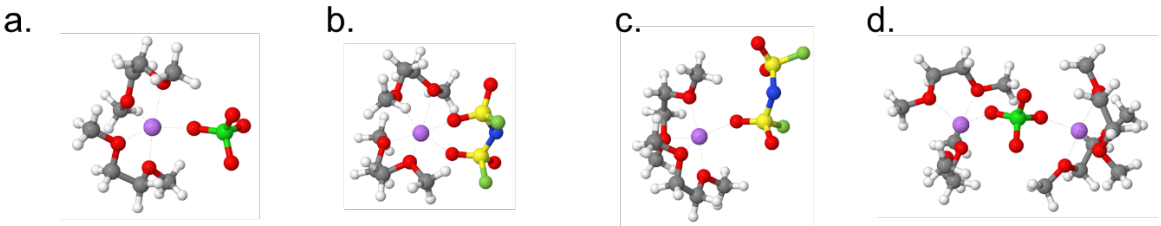

Figure S23. Representative Li^+ solvates for 0.91 M LiFSI and 0.27 M [TFP][ClO_4] in DME at 298 K.

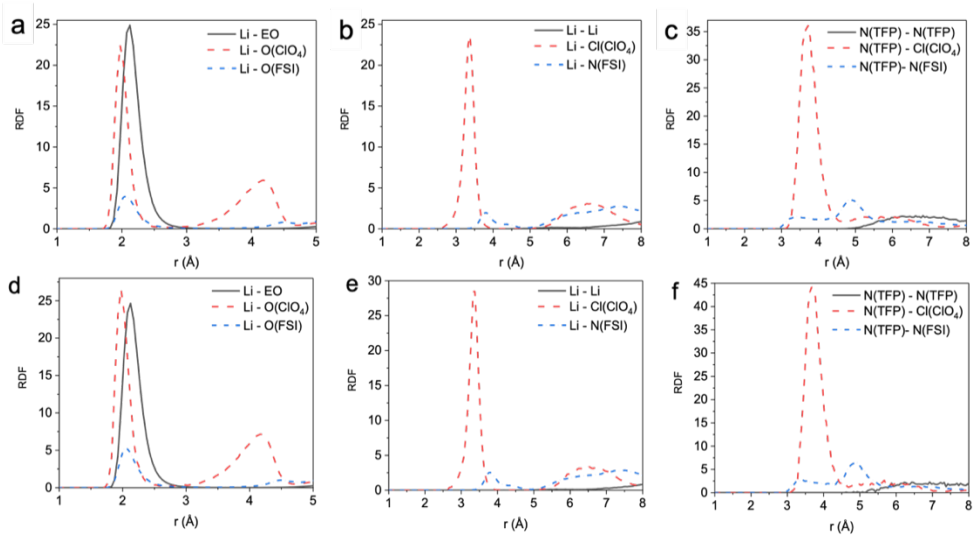

Figure S24. Radial distribution functions for (a-c) 0.91 M LiFSI and 0.27 M [TFP^+][$ClO4^-$] in DME and (d-f) 0.91 M LiFSI and 0.14 M [TFP^+][$ClO4^-$] in DME at 298 K.

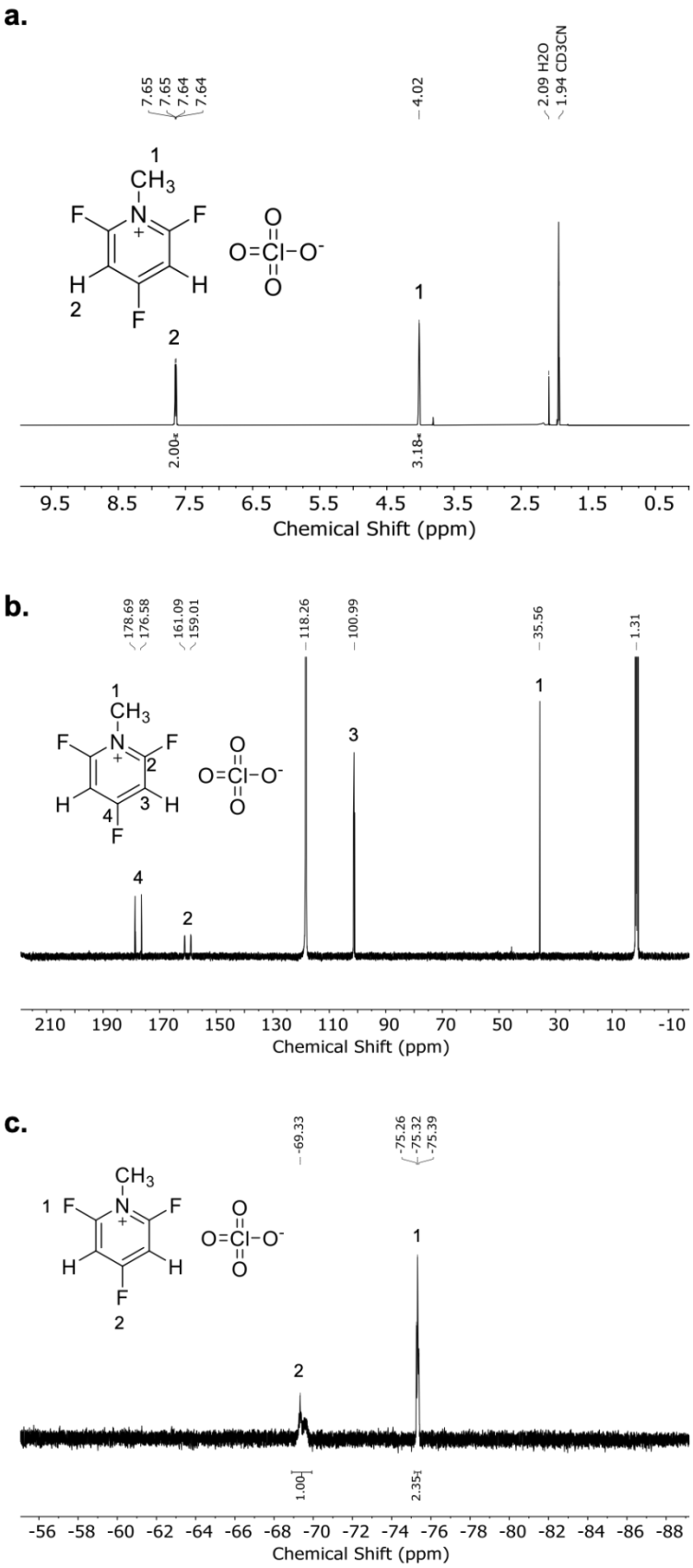

Figure S25. a. ^{1}H NMR spectrum of N-methyl-2,4,6-trifluoropyridinium perchlorate in acetonitrile-d_3. **b.** ^{13}C NMR spectra of N-methyl-2,4,6-trifluorocpyridinium perchlorate in acetonitrile-d_3. and **c.** ^{19}F NMR spectra of N-methyl-2,4,6-trifluoropyridinium perchlorate in acetonitrile-d_3.

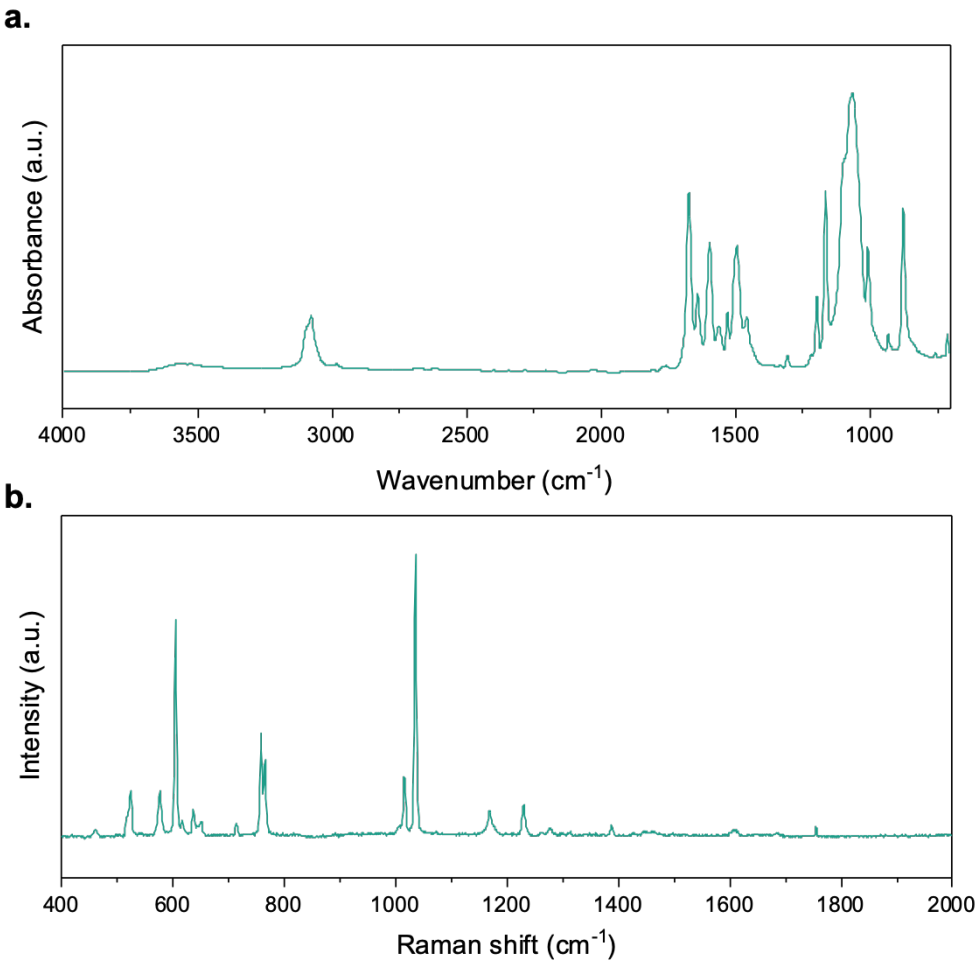

Figure S26. a. ATR-FTIR spectrum of crystalline TFP ClO_4. The FTIR spectrum was obtained by averaging 128 scans using a Vertex-70v spectrometer equipped with a narrow-band MCT detector and a Specac Golden Gate Diamond ATR accessory. **b.** Raman spectrum of crystalline TFP ClO_4. The Raman spectrum was obtained with 0.5% Laser power (785 nm Laser) and 20x magnification.

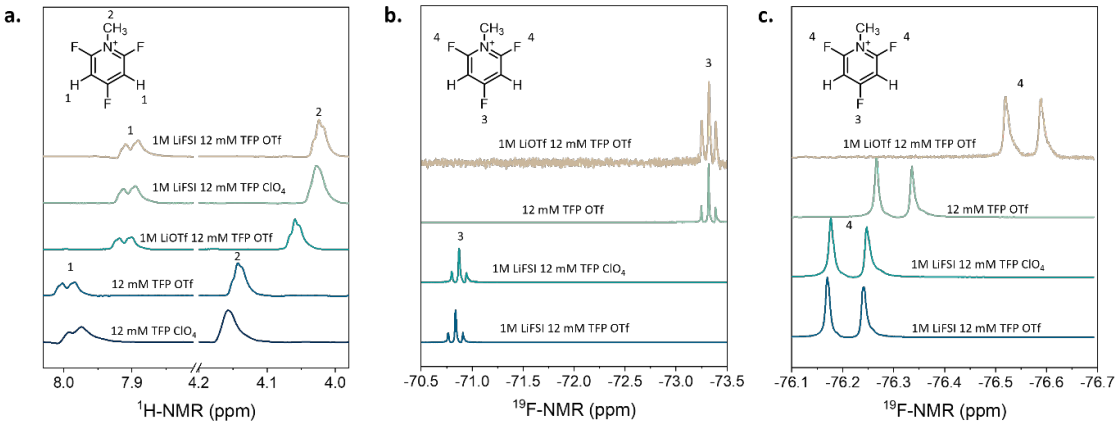

Figure S27. ^{1}H (**a**) and ^{19}F-NMR (**b**) spectroscopy of different electrolytes using indirect referencing to characterize the solvation environment of TFP. *For ^{1}H-NMR data processing, the DME signal was removed to deconvolute the additive signal.*

II. Supplementary Tables

Table S1. Surface elemental composition of different electrodes cycled in DME + 1M LiFSI with and without TFP.

Cu reduction DME + 1M LiFSI	Sputtering duration	
Element	18 s (at %)	72 s (at %)
O 1s	31.13	35.12
C 1s	36.58	37.22
S 2p	4.18	5.20
F 1s	6.51	9.28
N 1s	2.81	2.91
Li 1s	18.78	10.26
Sum	100	100
	F:C ratio	F:C ratio
	0.18	0.25

Cu reduction DME + 1M LiFSI + 18 mM TFP ClO_4	Sputtering duration	
Element	18 s (at %)	72 s (at %)
O 1s	12.37	8.94
C 1s	11.87	8.06
S 2p	1.04	0.25
F 1s	34.16	36.09
N 1s	0.36	1.13
Li 1s	40.2	45.53
Sum	100	100
	F:C ratio	F:C ratio
	2.88	4.48

Cu reduction DME + 1M LiFSI + 18 mM TFP triflate	Sputtering duration	
Element	18 s (at %)	72 s (at %)
O 1s	9.64	8.81
C 1s	6.6	4.64
S 2p	1.42	0.79
F 1s	29.95	31.14
N 1s	0.31	0.38
Li 1s	52.08	54.24
Sum	100	100
	F:C ratio	F:C ratio
	4.54	6.71

Li sample from symmetric cell DME + 1M LiFSI	Sputtering duration	
Element	18 s (at %)	72 s (at %)
O 1s	42.81	46.72
C 1s	36.85	35.14
S 2p	0.75	0.76
F 1s	1.81	2.6
N 1s	0	0
Li 1s	17.78	14.78
Sum	100	100
	F:C ratio	F:C ratio
	0.05	0.07

Li sample from symmetric cell DME + 1M LiFSI + 18 mM TFP ClO_4	Sputtering duration	
Element	18 s (at %)	72 s (at %)
O 1s	37.73	40.17
C 1s	31.47	22.39
S 2p	3.93	2.53
F 1s	4.79	6.75
N 1s	2.1	2.53
Li 1s	19.99	25.63
Sum	100.01	100
	F:C ratio	F:C ratio
	0.15	0.30

NCM sample from coin cell DME + 1M LiFSI	Sputtering duration	
Element	18 s (at %)	72 s (at %)
O 1s	24.94	23.52
C 1s	38.09	38.82
S 2p	4.33	4.5
F 1s	10.57	11.79
N 1s	3.15	4.49
Li 1s	18.91	16.89
Sum	99.99	100.01
	F:C ratio	F:C ratio
	0.28	0.30

NCM sample from coin cell DME + 1M LiFSI + 12 mM TFP ClO_4	Sputtering duration	
Element	18 s (at %)	72 s (at %)
O 1s	13.92	12.92
C 1s	53.75	44.94
S 2p	2.08	1.23
F 1s	19.51	18.85
N 1s	1.65	0.81
Li 1s	9.09	21.24
Sum	100	99.99
	F:C ratio	F:C ratio
	0.36	0.42

Table S2. The length of MD simulation trajectories, box size, the ion coordination, self-diffusion coefficients (D in 10^{-10} m^2 s^{-1}), conductivity (σ in mS cm^{-1}) and finite simulation cell correction to self-diffusion coefficients (ΔD^{FSC}) and conductivity ($\Delta\sigma^{FSC}$).

[TFP][ClO_4] concentration (M, mol L^{-1})	0.27	0.27	0.14	0.14
Temperature (K)	333	298	333	298
Length of equilibration runs (ns)	52	56	90	90
Length of production runs (ns)	307	180	340	398
Simulation box size (Å)	53.40	52.67	53.05	52.32
density (kg m^{-3})	983	1024	969	1011
D, DME (10^{-10} m^2 s^{-1})	17.2	9.0	18.1	9.6
D, FSI^- (10^{-10} m^2 s^{-1})	7.0	3.7	7.4	4.0
D, ClO_4^- (10^{-10} m^2 s^{-1})	5.4	2.4	5.9	2.9
D, TFP^+ (10^{-10} m^2 s^{-1})	5.5	2.9	6.2	3.3
D, Li^+ (10^{-10} m^2 s^{-1})	6.1	3.0	6.5	3.3
ΔD^{FSC} (10^{-10} m^2 s^{-1})	1.58	1.45	1.5	0.8
conductivity (σ) (mS cm^{-1})	17.8	13.0	16.6	14.4
$\Delta\sigma^{FSC}$ (mS cm^{-1})	4.0	2.7	4.0	3.2
Viscosity (mPa *s)	0.87	1.7	0.85	1.38
Inverse van Hove ratio	0.37	0.45	0.38	0.50
fraction of free Li^+, no O(FSI)<2.8 Å, O(ClO4)<2.8 Å	0.48	0.70	0.53	0.74
Number of EO (DME) within 2.8 Å of Li^+	4.69	5.29	4.80	5.36
Number of O(ClO_4^-) within 2.8 Å of Li^+	0.29	0.20	0.17	0.12
Number of O(FSI^-) within 2.8 Å of Li^+	0.46	0.18	0.54	0.24
Number of N(FSI^-) within 4.8 Å of Li^+	0.30	0.12	0.35	0.15
Number of Cl(ClO_4^-)within 4.8 Å of Li^+	0.28	0.20	0.17	0.12
Number of N(FSI^-) within 4.8 Å of TFP^+	0.50	0.44	0.58	0.54
Number of Cl(ClO_4^-) within 4.8 Å of TFP^+	0.51	0.61	0.29	0.34
Fraction of Free TFP^+	0.25	0.21	0.30	0.28

III. Supplementary Discussion

1. Discussion on LiFSI purity.

We used the LiFSI salt from TCI that has 98% purity (one of the impurities listed is Cl^-) for most experiments (unless indicated otherwise) because its use can reduce the cost of battery manufacturing. It is known that salt purity can significantly influence the extent to which parasitic processes occur when subjecting DME-based electrolytes to oxidizing potentials. As a result, LiFSI salt purity is known to substantially affect full cell cycling with high-voltage cathodes such as NCM811. This can be observed when a reference electrolyte (1M LiFSI) is used with NCM811 cathodes (**Figure S14 c and d).** However, we show the addition of TFP effectively inhibits the Al corrosion and DME decomposition regardless of the purity of LiFSI and enables a stable long-term cycling with high-voltage NCM811 cathodes (**Figure 3a** and **Figure S15**).

2. Molecular Dynamics Simulations TFP-containing electrolytes.

A. Simulation procedure: Molecular dynamics (MD) simulations were performed on two electrolyte compositions: 0.91 M LiFSI and 0.27 M [TFP][ClO_4] in DME and 0.93 M LiFSI and 0.14 M [TFP][ClO_4] in DME with a focus on providing insight into the Li^+ and TFP^+ coordination and ionic transport. A simulation cell comprised of 768 DME, 80 LiFSI and 24 [TFP][ClO_4] or 12 [TFP][ClO_4]. An increased concentration of [TFP][ClO_4] compared to experiments was used in MD simulations to ensure that a sufficient number of [TFP][ClO_4] are present in a simulation cell to allow formation of the TFP/ClO_4 and TFP/FSI - based aggregates during MD simulations. Investigation of two [TFP][ClO_4] concentrations allowed us to extrapolate the TFP^+ coordination numbers to lower [TFP][ClO_4] concentrations. Simulations were performed for 2 independent replicas 0.91 M LiFSI and 0.27 M [TFP][ClO_4] in DME and 3 independent replicas for 0.93 M LiFSI and 0.14 M [TFP][ClO_4] in DME electrolyte at 333 K and 298 K using different initial aggregation states. Replicas were pre-equilibrated for 6 - 13 ns at 363 K, following simulations at 333 K and 298 K. Total equilibration and production run lengths are shown in Table S2. The equilibration runs were performed in NPT ensemble, while production runs were performed in NVT ensemble. The local ionic environments for all replicas became similar during simulations, with the coordination numbers, self-diffusion coefficients, simulation cell linear length and density summarized in **Table S2**. The transport coefficients and finite simulation cell (FSC) corrections were extracted using previously discussed methodology.[1]

B. Discussion.

We performed molecular dynamics (MD) simulations to gain insight into the solvation structure of the TFP^+ cation. A snapshot of the MD simulation cell is shown in **Figure S21** together with the representative Li^+ solvates (**Figure S23**). At room temperature, the $Li^+(DME)_3$ solvates are prevalent: approximately 70 % of Li^+ are not coordinated by either ClO_4^- or FSI^- anions. High degree of LiFSI dissociation is consistent with Raman studies for 1M LiFSI in DME [2, 3] The rest of Li^+ participate in the Li^+/FSI^- and Li^+/ClO_4^- contact ion pairs (CIPs) shown in **Figure S23**.

Next, we examine the representative TFP^+ solvates shown in **Figure S22**. We observe a broad distribution of coordination environments that include the extended (1) positively charged, (2) negatively charged and (3) neutral aggregates. For the aggregates, the TFP^+ cations are more often bridged by ClO_4^- than FSI^- at higher additive concentration of 0.27 M [TFP][ClO_4] and more frequency bridged by FSI^- than ClO_4^- at 0.14 M lower [TFP][ClO_4] additive concentration. 28 % of TFP^+ cations are coordinated only by the DME solvent (without any anions in the TFP^+ first coordination shell) at 0.14 M [TFP][ClO_4] concentration and 21% at 0.27 M lower [TFP][ClO_4]. These TFP^+ cations are expected to

be attracted to the negative electrode and get reduced under reduction potentials (2.5 V from DFT calculations, see **Figure S11**).

Figure S24 shows the radial distribution functions (RDFs) for the respective electrolytes. We observe similar magnitudes of the first peak for Li^+ with ether oxygen atoms of DME [EO(DME)] and O(ClO_4^-), while Li-O(FSI) peak is significantly smaller indicating **strong affinity** of Li^+ to DME and ClO_4^- anions compared to FSI^-. The TFP^+-ClO_4^- RDF also shows a much higher first peak than that for TFP^+-FSI^-. Interestingly, both magnitude and widths of the first TFP^+/ClO_4^- peak are higher/larger than the corresponding Li^+/ClO_4^- RDF peak, indicating significantly stronger predisposition of the TFP^+ cation to form CIPs and AGGs than the corresponding lithium salts. We observe that while most of Li^+ (75 %) exist as free ions in agreement with the previous reports for 1M LiFSI in DME[4], a significant fraction of TFP^+ cations (~ 80 %) participate in CIPs and AGGs. Negatively charged AGGs are expected to be found at the positive electrode surface, while positive AGGs and free TFP^+ are expected to be found at the negative electrode surface. Thus, even at additive concentration of 0.14 M, we have 28 % of TFP^+ that are not coordinated to either anion. This indicates that there are **plenty of the positively charged TFP^+ to be electrostatically attracted at the negative lithium metal electrode** to participate in the reduction reaction and LiF formation, supporting the proposed mechanism.

Next, we also look at the changes in solvation at lower 0.14 M TFP concentrations using MD. While even these concentrations are still an order of magnitude higher than used in experiments, we could observe important trends related to the TFP^+ environments as summarized in **Table S2** for both [TFP^+][ClO_4^-] concentrations (0.14 M and 0.27 M). We see that while the TFP^+ - N(FSI^-) coordination number is relatively independent of the [TFP^+][ClO_4^-] concentration, the TFP^+ - ClO_4^- coordination number decreases with decreasing [TFP^+][ClO_4^-] concentration. Thus, at very small [TFP^+][ClO_4^-] concentrations, TFP^+ fraction interacting with anions will be primarily coordinated by FSI^- anions with a minor contribution from ClO_4^- despite the stronger TFP^+ - ClO_4^- peak in RDFs compared to the TFP^+ - N(FSI^-) RDF (**Figure S24c**).

The predicted conductivity at room temperature from MD simulations is in the range of 13 – 14 mS cm^{-1} before FSC correction and ~17 mS cm^{-1} after FSC correction, which is in good agreement with the experimental value of 16.9 mS cm^{-1} reported by Qian et al[5] and 15.2 mS cm^{-1} reported by Zhang et al[4]. MD-predicted viscosity of 0.93 M LiFSI and 0.14 M [TFP^+][ClO_4^-] in DME electrolyte is 1.42 mPa*s, which is similar to the experimental value of 1.25 - 1.42 mPa *s for 1M LiFSI in DME.[4] At lower additive concentrations of 0.14 M, DME was found to diffuse the fastest, followed by TFP^+ cation and ClO_4^-, FSI^- anion and Li^+. Inverse van Hove ratio (that is also often called ionicity) is 0.45-0.50 at room temperature, indicating moderate ionic correlations. It slightly increases with increasing conductivity but remains lower than a fraction of free Li^+ due to some ionic correlation through the low-dielectric-constant ether.

To sum up, MD simulations indicate that at 0.14 M of TFP the concentration of "free" TFP^+ (not coordinated by either anion) is 28 %. The TFP^+ cation has a stronger affinity to anions than the Li^+ cation, leading to the formation of a significant fractions of CIPs, charged and neutral AGGs at studied concentrations. It is important to emphasize that in our electrochemical experiments we work with TFP concentrations that are ~10-25 times **lower** than in the simulated electrolytes. Therefore, we anticipate the **fraction of free TFP^+ to be further increased in the case of 12 mM TFP** that we used in our electrochemical experiments, yielding a sufficient amount of free TFP^+ to be electrostatically attracted to anode surface to participate in SEI formation (in agreement with our EQCM-D results, **Fig. 2c**). *We should note that because simulations with of such dilute additive concentrations require the implementation of a much larger simulation box to obtain statistically relevant TFP coordination, we*

were unable to proceed with simulating with lower amounts of TFP due to the exceedingly high computational costs and time.

IV. Supplementary References

1. O. Borodin and G. D. Smith, *J. Phys. Chem. B*, 2009, **113**, 1763-1776.
2. J. D. Londono, B. K. Annis, A. Habenschuss, O. Borodin, G. D. Smith, J. Z. Turner and A. K. Soper, *Macromolecules*, 1997, **30**, 7151-7157.
3. Y. Chen, Z. Yu, P. Rudnicki, H. Gong, Z. Huang, S. C. Kim, J.-C. Lai, X. Kong, J. Qin, Y. Cui and Z. Bao, *J. Am. Chem. Soc.*, 2021, **143**, 18703-18713.
4. P. Zhang, H. Jin, T. Wang and M. Wang, *Electrochim. Acta*, 2018, **277**, 116-126.
5. J. Qian, W. A. Henderson, W. Xu, P. Bhattacharya, M. Engelhard, O. Borodin and J.-G. Zhang, *Nat. Commun.*, 2015, **6**, 6362.